Sub Topic: Fire

13th U.S. National Combustion Meeting
Organized by the Central States Section of the Combustion Institute
March 19–22, 2023
College Station, Texas

Experimental Studies on the Heat Flux of Individual Firebrands

Amy E. Mensch[1,*], *Savannah S. Wessies*[1], *Anthony Hamins*[1], *and Jiann C. Yang*[1]

[1]*Engineering Laboratory, National Institute of Standards and Technology, 100 Bureau Drive, Gaithersburg, MD, USA*

[*]*Corresponding author:* amy.mensch@nist.gov

Abstract: Every year, thousands of wildfires burn all over the world threatening lives and property in the wildland-urban interface. These wildland-urban interface fires spread by radiation, direct flame contact, or firebrand transport. Firebrand exposures are a significant cause of structural ignitions and have a significant impact at considerable distances from the fire. While firebrand ignition has been demonstrated in experiments, current fire models cannot accurately predict the threat of firebrand ignition to structures. One of the missing pieces for such a model framework is a thorough characterization of the heat transfer of glowing firebrands to structural surfaces. The current study uses a thin skin calorimeter to conduct measurements of the heat flux from individual firebrands. Generally, thin skin calorimeters are used to quantify only the radiative heat transfer to a surface from a fire exposure. In this work, we present results for the peak and total heat flux from a firebrand to an inert substrate in direct contact with the thin skin calorimeter. Using a propane burner, a disc-shaped piece of wood is used to generate consistent glowing firebrands, which are then placed on the thin skin calorimeter installed flush with the substrate. Previous studies on firebrand ignition of substrates have observed the effects on ignition propensity with variation in wind speed and wood type. The thin skin calorimeter experiments allow investigation of the impact of these factors on the firebrand heat transfer, which directly correlates to ignition. These experiments examine the effects of different firebrand wood types and wind speeds on peak heat flux, total heating, and duration of heating from the firebrand. These results will allow for the development of more accurate firebrand models and, in general, a better assessment of the hazard posed by firebrands in different scenarios.
Keywords: wildland-urban interface fires, firebrands, heat flux, thin skin calorimeter

1. Introduction

Wildland-urban interface (WUI) fires represent a growing international threat to lives and property from rural to urban communities. WUI fires can generate hazardous conditions that are difficult to predict and control, leading to substantial loss of life, destruction of structures and wildland, and even poor air quality far from the location of the fire. In the United States from 2011 to 2021, there were 15 WUI fires that each caused losses of more than $100 million [1]. With 85 deaths, the 2018 Camp Fire was the most destructive and deadly fire in California history. The fast moving Camp Fire was driven by high winds and characterized by long range spotting, up to 6.3 km [2]. Spot fires generated by firebrands transported ahead of the fire front are a significant driver of WUI fire spread and cause of structure ignitions [3].

Firebrands are fragments of burning material that break off from burning vegetation or structures and are lofted by the wind. Firebrands can travel great distances and ignite structures when the firebrands deposit and collect on structural components or the surrounding landscape. The transient phenomenon of firebrand ignition involves a complex combination of heat transfer processes

between the firebrands, the substrate and the surroundings. Nazare et al. [3] presents a comprehensive review of the current understanding of firebrand ignition mechanisms of wood substrates. Ignition criteria for exposure to a constant radiant heat flux can be characterized by the critical ignition temperature, critical heat flux, or critical mass loss rate of the substrate, and the critical heat flux represents the lowest criterion of constant heat flux for ignition [3].

Several previous studies related to firebrand ignition mechanisms have focused on measurements of the firebrand heat flux to a substrate, often for firebrand piles [4–8], and a few for individual firebrands [4, 9]. Most investigations expose the firebrands to flow velocities up to 2 m/s, which are lower than wind speeds in a WUI fire, but are representative of velocities close to the surface where firebrands deposit. Different wood types and geometries to generate firebrands have been explored across previous investigations, including Scottish softwood pellets [6], birch cylinders [4, 7, 8], and oak cuboids and cylinders [9].

The following investigations explored the effects of pile size, and firebrand geometry, material, or condition on the peak net heat flux. Hakes et al. [4] compared the heat flux from individual and piles of cylindrical birch firebrands using a water-cooled heat flux gauge. They considered the effects of firebrand diameter, pile mass, and wind on both the peak heat flux and total heat released. The heat flux gauge measurements for individual firebrands were less than 20 kW/m^2 and lower than that of firebrand piles. Tao et al. [5] used a water-cooled heat flux gauge to measure the peak heat flux from piles of different firebrand types, including birch cylinders of different sizes, birch discs of different thicknesses, eucalyptus sticks of different lengths, and pine bark. The authors investigated how the bulk density of the piles affected the peak heat flux and found different trends between the machined birch firebrands and the realistic firebrands. Among the birch firebrand piles, they observed higher peak heat flux with higher pile bulk density. Thomas et al. [6] evaluated differences in the measured heat flux from firebrand piles generated in an oven at different temperatures. Peak net heat fluxes were determined from an inverse heat transfer model and from measured substrate temperatures. They reported peak net heat fluxes between 4 kW/m^2 and 9 kW/m^2, which depended primarily on the oven temperature used for the firebrand generation. Different geometries of individual oak firebrands were considered by Bearinger et al. [9] who measured the firebrand heat flux distributions using inverse heat transfer and infrared thermography on the underside of the substrate. They used six distinct cuboid and cylinder geometries, nearly all with the same projected area and masses between 0.7 g and 1.2 g. The maximum heat flux measurements were reported for both the peak location (0.4 mm resolution) and the average over the firebrand projected area. Peak local heat fluxes ranged from 30 kW/m^2 to 105 kW/m^2, whereas average heat fluxes measured from 14 kW/m^2 to 23 kW/m^2.

Measurements of the time-dependent heat flux from individual firebrands can improve our understanding of firebrand heat transfer and their ignition threat. The current study uses a thin skin calorimeter to investigate the net heat flux of individual disc firebrands with varying wood materials and flow velocities. The four wood types in this study are native to forests across the USA and represent both hardwoods and softwoods, and lower and higher wood densities. This study investigates the effects of wood type and density on firebrand heat flux to better understand the hazard for WUI communities.

2. Experimental Methods

A copper thin skin calorimeter (TSC) with a thickness, δ, of 0.552 mm and a diameter, D, of 19.1 mm was embedded into the surface of a ceramic fiber board substrate, with a thickness of 25.4 mm, as shown in Figure 1a. The firebrand heat flux was based on the rate of change in temperature of the TSC, dT_{TSC}/dt, which was measured by attaching K-type thermocouple (TC) wires to the underside of the TSC. The temperature of the TSC was assumed to be uniform, as the Biot number was estimated to be on the order of 10^{-5} based on δ and on the order of 10^{-3} based on D. The energy balance on the TSC is shown in Figure 1b, where the net heat transfer rate from the firebrand to the TSC, q_{net}, was a sum of the thermal storage, q_{stor}, and conductive losses from the TSC to the insulating substrate, q_{cond}. The TSC was designed to have the same diameter as the deposited firebrand in order to neglect convective and radiative heat losses from the top of the TSC.

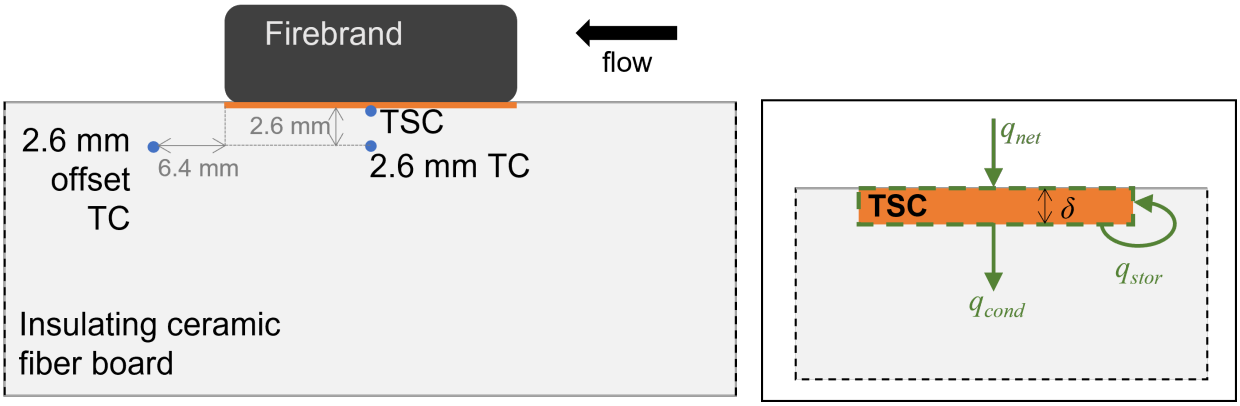

(a) (b)

Figure 1: Diagrams of (a) the TSC system and TC locations and (b) the thermal energy balance on the TSC.

Equation 1 defines the net heat flux from the firebrand to the TSC, q''_{net}, where A_{surf} was the surface area of the TSC exposed to the firebrand ($\pi D^2/4$), ρ was the density of copper (8960 kg/m^3), and c_p was the specific heat of copper (0.385 kJ/kgK).

$$q''_{net} = \frac{q_{stor} + q_{cond}}{A_{surf}} = (\rho c_p \delta)_{TSC} \frac{dT_{TSC}}{dt} + q''_{cond} \tag{1}$$

A second order central difference scheme was used to calculate dT_{TSC}/dt from the TSC temperature, recorded at a rate of 6 Hz. Two additional TCs installed within the substrate, as shown in Figure 1a, were used to estimate q_{cond} from Fourier's Law. The diameter of the TC beads was approximately 0.5 mm. The vertical component of q_{cond} was $-k_s A \Delta T/\Delta x$, where k_s was the thermal conductivity of the substrate (0.068 W/mK), A was the heat transfer surface area (A_{surf}), ΔT was the temperature difference between the TSC and the 2.6 mm TC, and Δx was 2.6 mm. Although much smaller, the lateral component of q_{cond} was computed and summed with the vertical component. The lateral component of q_{cond} was computed using $A = \pi D$ x 2.6 mm, the temperature difference between the two embedded TCs in Figure 1a, and 6.4 mm for Δx. The uncertainty in the

peak q''_{net} was estimated to be $\pm$ 6 % to $\pm$ 15 %, with the largest contribution from the numerical calculation of dT_{TSC}/dt, as shown for two representative experiments at 0.6 m/s in Table 1.

Table 1: Contributions to uncertainty in peak q''_{net} from the uncertainties in δ and dT_{TSC}/dt, with a coverage factor of 2 used for the combined uncertainty, for two representative experiments at 0.6 m/s.

Type	**Uncert. contribution due to:**			**2 $\times$ Comb.**
	δ (%)	dT_{TSC}/dt (%)	$q''_{cond,exp}$ (%)	**Uncert.** (%)
Oak	1.2	2.5	0.30	6
Birch	1.2	7.4	0.25	15

Two different flow conditions were imposed in the current study using a single-pass wind tunnel depicted in Figure 2. The flow velocity 12.7 mm above the TSC was measured with a hot wire anemometer before each experiment. The average velocities were 0.6 m/s and 1.0 m/s, representing a low and medium flow condition compared to similar firebrand studies. For both average velocities, the standard uncertainty for a 95 % confidence interval was 0.05 m/s.

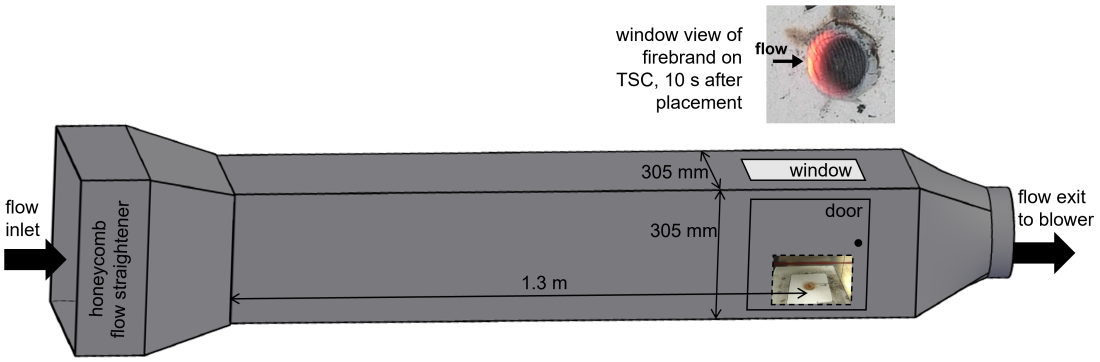

Figure 2: Depiction of the single-pass wind tunnel to generate the flow conditions of between 0.6 m/s and 1.0 m/s. The TSC and substrate, installed flush with the floor, are shown behind the door used to deposit glowing firebrands.

Firebrands were generated from disc shaped samples made of four different wood types, which were oak, western red cedar, pine, and birch. The wood discs were cut from 25.4 mm diameter dowels to a thickness of 8.4 mm and completely dried in a 110 °C oven. Before each experiment, the dried wood disc was weighed and then ignited through exposure to direct flame for 10 s over a propane burner surrounded by a chimney. The wood disc remained in the chimney until the flame self-extinguished. Then the wood disc was picked up with tongs and placed on the TSC in the wind tunnel using the side door shown in Figure 2. Data was collected until the TSC temperature cooled back to a similar temperature as the substrate. Then the remnants of the firebrand were removed from the TSC to a mass balance to obtain the post-test mass. Each wood type was tested for three repeat experiments at both flow conditions.

3. Results and Discussion

The average initial masses of the individual wood discs after drying but before firebrand generation are shown in Table 2 for each wood type. The calculated density is also shown, using the average mass and volume calculated from the disc diameter and thickness. While oak has the highest density, the density of cedar is much lower, and the densities for pine and birch are just slightly lower than oak. The percent mass consumed is also included in Table 2 for both flow conditions. The percent mass consumed shows significant differences between some of the wood types, with oak having the lowest, followed by cedar, and then pine and birch with the highest. There is almost no difference in percent mass consumed between 0.6 m/s and 1.0 m/s.

Table 2: Mass, density, and percentage of the mass consumed during generation and testing for the four different wood types, averaged over the three repeats.

	Mean Initial	**Mean Density**	**Mean Mass Consumed** (%)	
Wood Type	**Mass** (g)	(kg/m^3)	*0.6 m/s*	*1.0 m/s*
Oak	2.714	639	81 ± 2	82 ± 3
Cedar	1.468	346	89 ± 1	89 ± 1
Pine	2.409	567	95 ± 1	95 ± 1
Birch	2.333	549	95 ± 2	95 ± 2

Variation in burning among the different wood types is evident in Figure 3, which shows images of the firebrand under the 0.6 m/s flow condition at four times after placement on the TSC for a representative experiment for each wood type. During generation the firebrands shrink from their original diameter of 25.4 mm to approximately the same diameter as the TSC, 19.1 mm, as shown in the first column of images at 0 s at deposition. Pine shrinks the most, while oak shrinks the least. The deposition images show the most glowing combustion around the entire edge of the firebrands, except for oak, which has almost no visible glowing. At 30 s, it can be seen that the glowing has reduced and is occurring only at the leading edge of the firebrand, which has the best access to oxygen to support smoldering. The glowing is sustained longest, past 90 s, for pine and birch, which is consistent with their results for the highest percent mass consumed. Particularly with the pine test, continued shrinkage of the firebrand is observed on the TSC, as smoldering regions convert char to ash that can easily detach from the firebrand.

A q''_{net} profile is given in Figure 4 for the cedar firebrand experiment shown in Figure 3 in the 0.6 m/s flow condition. q''_{net} is the sum of the q''_{stor} measured by the TSC and the q''_{cond} loss measured by the thermocouples embedded in the substrate. Initially, q''_{stor} dominates q''_{net} through the peak that occurs in the first 2 s. By 30 s, the firebrand smoldering has slowed, as seen in Figure 3, and the q''_{stor} crosses below q''_{cond}, meaning at that time the additional heating of the TSC from the firebrand has become less than the heat transfer from the TSC to the substrate. After 50 s, q''_{stor} becomes negative, which means the TSC is cooling, but q''_{net} is still positive due to the contribution from q''_{cond}. Although q''_{cond} has a negligible contribution to the initial peak q''_{net}, the inclusion of q''_{cond} significantly increases the the total heating and duration of heating of the substrate.

The profiles across both flow conditions and all wood types have similar shapes and trends, although the peak q''_{net} magnitude and timing varies. Figure 5 shows the first 10 s of representative q''_{net} profiles for all wood types at the 0.6 m/s flow condition. These are the same experiments depicted in Figure 3. The q''_{net} peak values are very similar for cedar, pine and birch, which also show

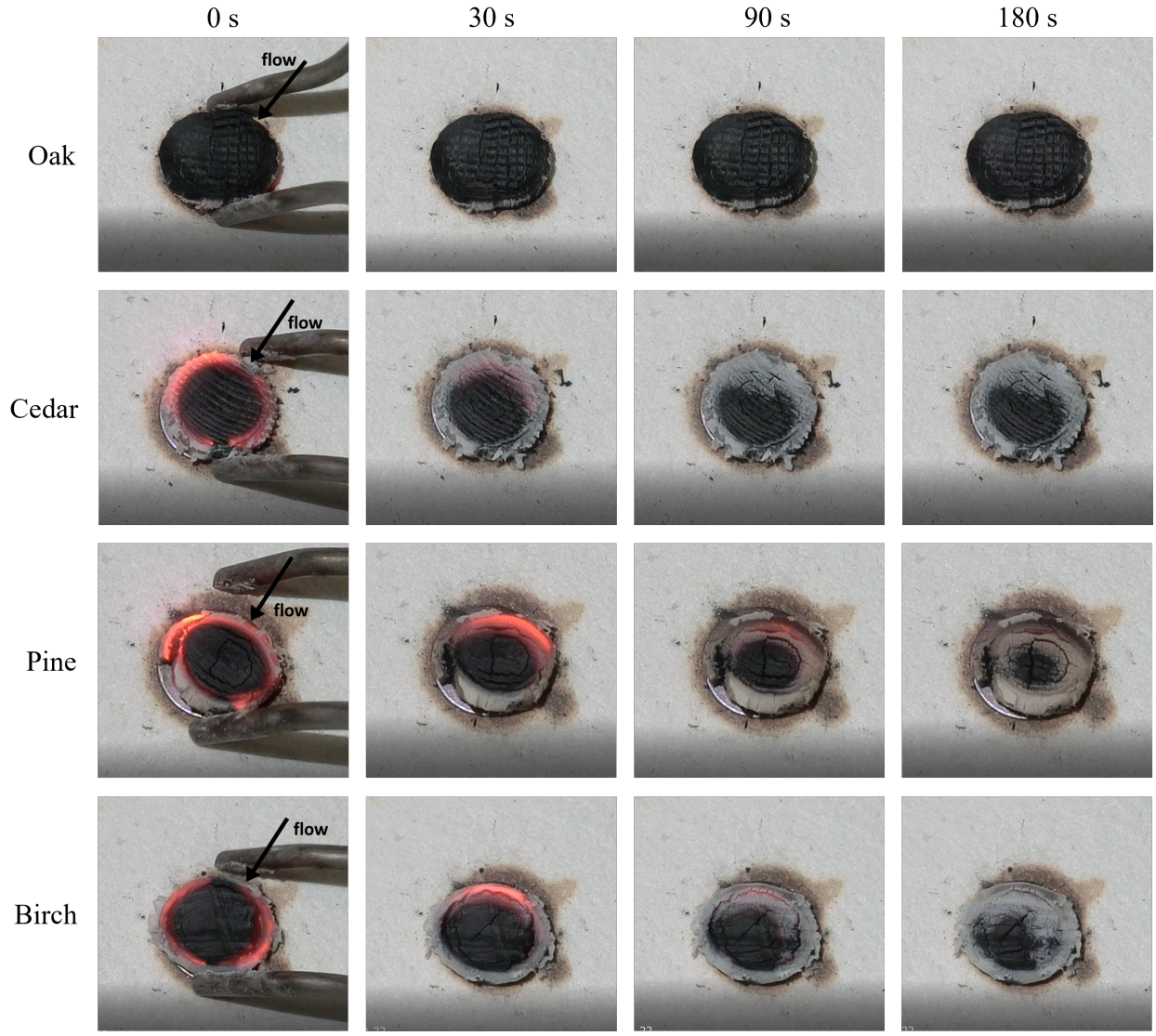

Figure 3: Images showing the progression of the firebrand during the first 180 s of a representative experiment for each wood type under the 0.6 m/s flow condition.

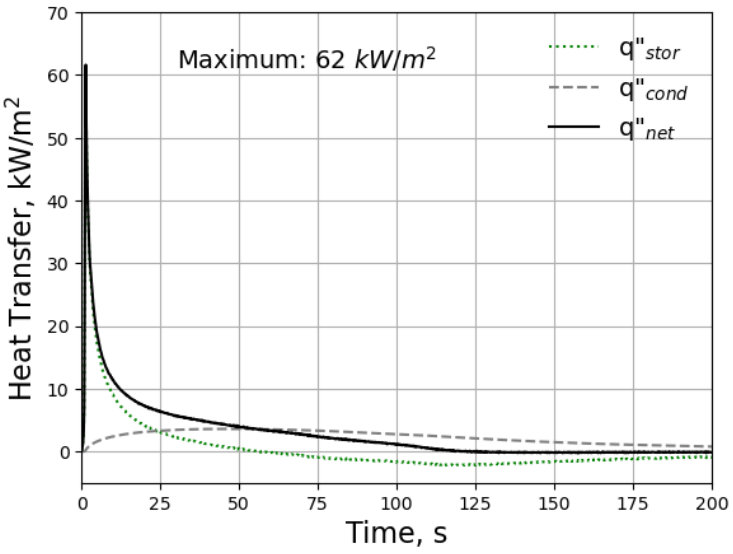

Figure 4: Heat flux profiles for a cedar firebrand at the 0.6 m/s flow condition, corresponding to the firebrand images shown in the second row of Figure 3.

similar extent of glowing and ash formation in Figure 3. The peak q''_{net} in Figure 5 is 60 kW/m^2 for pine, 74 kW/m^2 for birch, and 62 kW/m^2 for cedar, and all occur between 1.0 s and 1.3 s. The peak q''_{net} for oak is significantly lower, 40 kW/m^2, consistent with the lack of visible glowing or ash formation in Figure 5. The peak for this oak experiment is also relatively delayed, occurring at 2.3 s. The q''_{net} profiles of cedar, pine, and birch are similar in shape to the single birch firebrand heat flux profile measured by Hakes et al. [4] using a water-cooled heat flux gauge.

Figure 6 shows the average values of peak q''_{net} measured at both flow conditions for each wood type. The measurement uncertainty in the peak q''_{net} measurement is given in Table 1, $\pm$ 15 % for birch and $\pm$ 6 % for oak. The error bars in Figure 6 represent the 95 % confidence interval of the mean of the three replicates for each case. There is not a significant difference in the peak q''_{net} at the two flow conditions. Considering the error bars, there is overlap between the peak q''_{net} from the different wood types as well. The exception is oak, whose peak q''_{net} is measurably lower than both cedar and birch. The error bars indicate that the peak q''_{net} for oak and cedar varies less compared to pine and birch.

In previous studies, peak net heat flux values (averaged over the initial firebrand area) for individual firebrands have ranged from 10 kW/m^2 to 30 kW/m^2 for flow conditions between 0 m/s and 2 m/s [4, 9]. Our measurements are higher, with peaks from individual experiments ranging between 35 kW/m^2 to 80 kW/m^2. However, this range of values is similar to peak values measured by a water-cooled heat flux gauge for firebrand piles [4]. It is possible that the experimental setups that use a water-cooled heat flux gauge or metal substrate may have a quenching effect on a single firebrand, and result in a lower measured peak heat flux.

The total heat transfer from the firebrand to the substrate is found by integrating the q''_{net} profile until the q''_{net} profile is no longer positive. The time until q''_{net} becomes negative is the duration of heating from the firebrand. The average total heating per unit area for each wood type and flow condition are given in Figure 7. The error bars represent the 95 % confidence level in the mean. Like q''_{net}, none of the wood types show a significant difference in total heating with flow

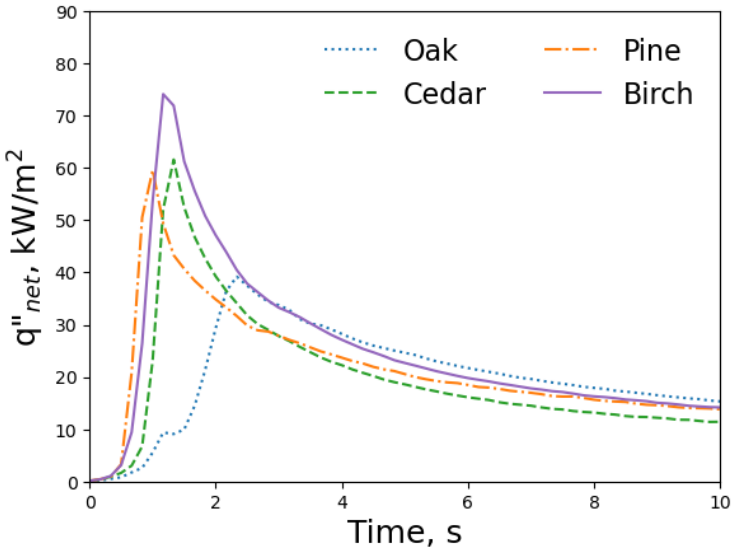

Figure 5: Representative net heat flux profiles for each wood type at the 0.6 m/s flow condition.

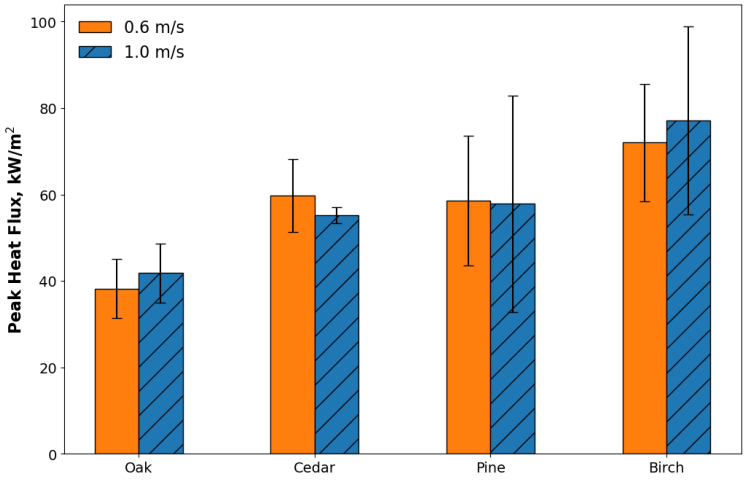

Figure 6: Summary of the average values measured for peak heat flux (q''_{net}) for all wood types at both flow conditions. Error bars represent the 95 % confidence in the mean value from the three repeat experiments.

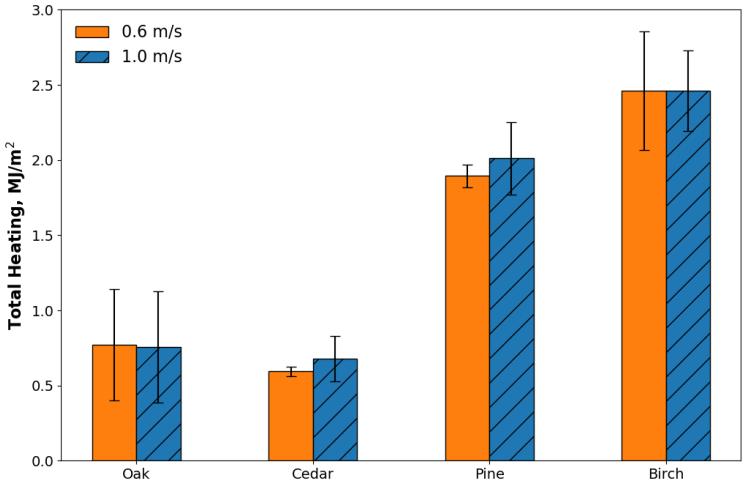

Figure 7: Summary of the average values of total heating measured for all wood types at both flow conditions. Error bars represent the 95 % confidence in the mean value from the three repeat experiments.

condition. There is more of a distinction in total heating between wood types, with oak and cedar having average total heating values less than 1 MJ/m^2, and pine and birch having average total heating values around 2 MJ/m^2 to 2.5 MJ/m^2. The duration of heating shows similar trends with flow condition and wood type, which is expected due to the dependence of total heating on the duration of heating. In order of shortest to longest, the average duration of heating values were 127 s for cedar, 179 s for oak, 406 s for pine, and 459 s for birch. For both flow conditions, the total heating appears somewhat correlated with the percent mass consumed, reported in Table 2, which also has oak and cedar with lower values compared to pine and birch. Variations in total heating and in percent mass consumed could be related to the wood's grain structure and chemical composition and their impact on the smoldering efficiency. Hakes et al. [4] found that for the same types of firebrands, the total heating was linearly correlated to the firebrand pile mass. The total heating is dependent on the total energy released, which is dependent on the mass of wood consumed.

4. Conclusions

A thin skin calorimeter was used to measure the time-resolved heat flux from individual firebrands deposited on a substrate. Measurements were obtained for glowing firebrands exposed to wind conditions of 0.6 m/s and 1.0 m/s. The firebrands were generated from oak, western red cedar, pine, and birch discs. Peak heat flux and other quantities that may be useful to quantify the firebrand ignition hazard, including the percent mass consumed, total heating, and duration of heating, were all reported. The results showed no significant differences between the two velocities considered in this study for percent mass consumed, peak heat flux, total heating, and duration of heating. Future work will investigate the effect of additional variation in wind velocity, as this is expected to impact at least the total heating from firebrands. Peak heat flux occurred consistently between 1 s and 2.3 s after firebrand deposition. Although there was some variation in each wood type's average peak heat flux, there was much overlap between the uncertainties. The one wood type

with a lower average peak heat flux, oak, also showed visibly less glowing compared to the other wood types from the moment of deposition. The related quantities of percent mass consumed, total heating, and duration of heating varied between the wood types, with lower values for oak and cedar, and higher values for pine and birch. Increased total heating was found for increasing wood density, with the exception of oak, which had the highest density, but the lowest total heating. It is likely that differences in wood structure and chemistry are impacting the smoldering efficiency and subsequent heat transfer to the substrate.

References

[1] S. G. Badger, Large-Loss Fires and Explosions in the United States in 2020, National Fire Protection Association, 1 Batterymarch Park, Quincy, MA (2021).

[2] A. Maranghides, E. Link, W. Mell, S. Hawks, M. Wilson, W. Brewer, C. Brown, B. Vihnaneck, and W. D. Walton, A Case Study of the Camp Fire – Fire Progression Timeline, NIST Technical Note TN 2135, National Institute of Standards and Technology, Gaithersburg, MD (Jan 2021), DOI: 10.6028/NIST.TN.2135.

[3] S. Nazare, I. Leventon, and R. Davis, Ignitibility of Structural Wood Products Exposed to Embers During Wildland Fires: A Review of Literature, NIST Technical Note TN 2153, National Institute of Standards and Technology, Gaithersburg, MD (April 2021), DOI: 10.6028/NIST.TN.2153.

[4] R. S. Hakes, H. Salehizadeh, M. J. Weston-Dawkes, and M. J. Gollner, Thermal characterization of firebrand piles, Fire Safety Journal 104 (2019) 34–42.

[5] Z. Tao, B. Bathras, B. Kwon, B. Biallas, M. J. Gollner, and R. Yang, Effect of firebrand size and geometry on heating from a smoldering pile under wind, Fire Safety Journal 120 (2021) 103031.

[6] J. C. Thomas, E. V. Mueller, and R. M. Hadden, Estimating net heat flux from surrogate firebrand accumulations using an inverse heat transfer approach, Advances in forest fire research 2018 (2018) 769–779. DOI: 10.14195/978-989-26-16-506_84.

[7] H. Salehizadeh, R. S. P. Hakes, and M. J. Gollner, Critical Ignition Conditions of Wood by Cylindrical Firebrands, Frontiers in Mechanical Engineering 7 (2021) 630324.

[8] F. Richter, B. Bathras, J. Barbetta Duarte, and M. J. Gollner, The Propensity of Wooden Crevices to Smoldering Ignition by Firebrands, Fire Technology 58 (2022) 2167–2188.

[9] E. D. Bearinger, J. L. Hodges, F. Yang, C. M. Rippe, and B. Y. Lattimer, Localized heat transfer from firebrands to surfaces, Fire Safety Journal 120 (2021) 103037.